Available online at www.sciencedirect.com
SCIENCE DIRECT®
Biomaterials 27 (2006) 1988–2000
Biomaterials
www.elsevier.com/locate/biomaterials

Fatigue and life prediction for cobalt-chromium stents: A fracture mechanics analysis

Ramesh V. Marrey[a], Robert Burgermeister[a], Randy B. Grishaber[a], R.O. Ritchie[b,*]

[a]*Cordis Corporation, a Johnson & Johnson company, 7 Powder Horn Drive, Warren, NJ 07059, USA*
[b]*Materials Sciences Division, Lawrence Berkeley National Laboratory and Department of Materials Science and Engineering, University of California, Berkeley, CA 94720-1760, USA*

Received 23 June 2005; accepted 9 October 2005
Available online 2 November 2005

Abstract

To design against premature mechanical failure, most implant devices such as coronary and endovascular stents are assessed *on the basis of survival*, i.e., if a fatigue life of 10^8 cycles is required, testing is performed to ascertain whether the device will survive 10^8 cycles under accelerated in vitro loading conditions. This is a far from satisfactory approach as the safety factors, which essentially tell you how close you are to failure, remain unknown; rather, the probability of fatigue failure should instead be assessed *on the basis of testing to failure*. In this work, a new damage-tolerant analysis of a cardiovascular stent is presented, where the design life is conservatively evaluated using a fracture mechanics methodology. In addition to enabling estimates of safe in vivo lifetimes to be made, this approach serves to quantify the effect of flaws in terms of their potential effect on device failure, and as such provides a rational basis for quality control.

Keywords: Fracture mechanics; Fatigue; Coronary stents; Life prediction

1. Introduction

Currently, more than one million stents are implanted in human arteries each year to counteract the effects of atherosclerosis. Indeed, the market for endo- and cardiovascular stents is projected to exceed $7 billion by the year 2006. Although mechanical failure of such devices will not necessarily threaten the life of the patient, it is an undesirable event that should be avoided. For balloon-expandable stents, which are manufactured primarily from austenitic stainless steel (e.g., AISI 316L) or cobalt–chromium (Co–Cr) alloys (e.g., Haynes®[1] 25), structural damage can occur from outright fracture of the stent, for example due to the loading imposed by over expansion, or over time due to fatigue failure from the physiological pulsatile contact pressures at the artery vessel walls, both instances where the presence of pre-existing flaws or imperfections in the metal can markedly increase the probability of premature failure. Cyclic fatigue failure is particularly important as the heart beats, and hence the arteries "pulse", at typically 70 plus times a minute—some 40 million times per year—necessitating that these devices are designed to last in excess of 10^8 loading cycles for a 10-year life.

To design against such fatigue failures, stents are currently assessed *on the basis of testing for survival*, i.e., if a design life of 10^8 cycles is required, testing is performed to ascertain whether the stent will survive 10^8 cycles under accelerated simulated physiological loading. This is an inadequate approach, as the safety factors, which essentially tell you how close you are to failure, remain unknown. Indeed, this approach to fatigue design is quite unlike that used in most other fields of engineering, e.g., in automobile or aerospace applications, where the probability of fatigue failure is instead assessed *on the basis of testing to failure*. This is typically achieved using one of two

*Corresponding author. Tel.: +1 510 486 5798; fax: +1 510 486 4881.
E-mail address: roritchie@lbl.gov (R.O. Ritchie).
[1]Registered Trademark of Haynes International, Inc.

0142-9612/$ - see front matter © 2005 Elsevier Ltd. All rights reserved.
doi:10.1016/j.biomaterials.2005.10.012

methodologies: (1) the traditional stress/strain-life ($S-N$) approach, where design and life prediction rely on experimentally determined relationships between the applied stress or strain and the total life of the component, and (2) the damage-tolerant or fracture-mechanics approach, where life is computed in terms of the time or number of cycles to propagate the largest pre-existing flaw to failure. Although the simpler $S-N$ approach is more widely used, particularly for small components, the fracture-mechanics approach offers many distinct advantages, in that (i) it is invariably more conservative, (ii) it enables a quantitative evaluation of the damaging effect of flaws or defects in the material, and (iii) it provides a rational basis for quality control of the product. A good example of this is in the design, life prediction and quality control of prosthetic heart valve devices [1,2].

In the present work, we develop a new methodology for quantitatively predicting the fatigue life of a new cardiovascular stent fabricated from the L-605 Co–Cr alloy. Our approach is to base the primary fatigue-life assessment on a traditional, yet conservative version of an $S-N$ analysis, and to further use fracture mechanics in order to evaluate the role of pre-existing flaws. In the latter analysis, we quantitatively assess the severity of microstructural flaws observed on expanded stents, in terms of the propensity of the flaw to propagate and lead to in vivo failure of the stent when subjected to cyclic systolic/diastolic pressure loads within the implanted artery. Specifically, stress-intensity factors for flaws of differing lengths in the stent structure are characterized, and the difference in the stress intensities associated with the systolic and diastolic pressure loads is compared with the fatigue crack-growth thresholds to determine the level of flaw severity. Experimental data for fatigue crack-growth rates for the L605 Co–Cr alloy are then used to determine the remaining stent life based on the loading cycles required to propagate the flaw to a critical size, where stent failure would be predicted to occur. The analysis takes into consideration the effect of so-called small cracks [3,4] in order to estimate the fatigue life of the stent as a function of the size of any pre-existing flaws, and as such provides a quantitative basis for a quality-assurance assessment of the stent. It should be mentioned that in the context of this work, "stent failure" is indicative of local structural instability under cyclic loading conditions that would lead to strut fracture.

2. Material

The stent in question was manufactured from wrought Co–Cr alloy, commonly referred to as L-605 (UNS R30605) that is compositionally equivalent to Haynes 25. The use of this material enables a reduction in stent wall thickness relative to traditional stainless steels (e.g., AISI 316L) while retaining adequate visibility under fluoroscopy, i.e., clinical X-ray-based imaging. The solid-solution alloy evaluated is nominally comprised of 20 wt% chromium, 15 wt% tungsten, 10 wt% nickel, 1.5 wt% manganese, 0.1 wt% carbon, 3 wt% iron, trace amounts of silicon, phosphorus and sulfur, and the balance consisting of cobalt.

Table 1
Physical and mechanical properties of L-605 Co–Cr alloy

Young's modulus, E [9] (GPa)	0.2% offset yield strength, σ_y (Mpa)	Tensile strength, σ_u (MPa)	Fatigue endurance strength[a], $\Delta\sigma_e/2$ (MPa)
243	547	1449	207

[a]Defined at $R=-1$, where R, the load (or stress) ratio, is the ratio of minimum to maximum loads (or stresses) in the fatigue cycle.

The Co–Cr alloy was produced by a combination of vacuum-induction melting and vacuum-arc reduction molten state processing of the constituent elemental raw materials into a chemically homogenized billet. The primary ingot was then thermomechanically processed to round-bar form through a series of consecutive hot rolling reduction steps. From a nominal starting bar size of the order of 25 mm in diameter, the round-bar was 'gun-drilled' to form a heavy walled, tubular form (commonly referred to as a 'tube hollow'). The work-in-progress raw material was further reduced to the intended final outer diameter and wall dimensions by use of sequential cold finishing reductions and subsequent in-process annealing steps. Final mechanical properties of the finished raw material were achieved by thermally annealing in vacuo followed by a tube-straightening process.

The mechanical properties of the L-605 alloy were measured from standard uniaxial tensile tests, with the exception of endurance strength which was measured from rotary-beam testing of wire, as described in Section 4. The uniaxial tensile tests were performed on tubular specimens with outer diameter of 1.47 mm at a displacement rate of 13 mm/min. The tested tubes were extracted from batches that were eventually used to process the stent structure. The tubing microstructure consisted of a relatively uniform, equiaxed grain-size that was experimentally confirmed to be ~30 μm or less (i.e., ASTM E112 grain-size of 7 or finer) [5]. The tubing used in this treatment is consistent with that used in other clinically relevant devices.

The stent specimens were processed by laser cutting the intended geometry onto the surface of the tubing. Additionally, the as-cut surfaces were then electrochemically processed in a manner consistent with industrially accepted processes that utilize both acidic and caustic baths to achieve a near uniform, electropolished surface finish (i.e., surface roughness target, R_a, of 0.2 μm or finer). All stent specimens were evaluated against relevant internal processing standards on both a visual, functional and dimensional basis prior to subsequent experimental utilization.

The wire specimens used to determine the fatigue endurance strength were fabricated by conventional 'cold-finishing' wire drawing methods. Significant effort was made to ensure that the composition and the primary melt processing of the originating ingot for the wire stock was equivalent to that of the tubing stock investigated. In-process and final annealing treatments were used to achieve equivalent mechanical properties in the drawn wire lot to the evaluated tubing stock in terms of uniaxial yield strength, tensile strength and terminal ductility. The surface finish of the wire specimens was consistent with that of the evaluated tubing stock.

Statistical analysis of the experimental results gathered was used to determine the conservative values shown in Table 1 for yield and ultimate tensile strengths and the fatigue endurance strength of the material. The Young's modulus value was taken from Ref. [6].

3. Stress analysis

In order to perform an initial stress-life analysis for fatigue loading in a simulated in vivo environment, the steps involved in preparing and deploying an interventional

stent consistent with clinical practice need to be addressed. First, the fabricated stent is loaded onto the intravascular delivery system (i.e., balloon catheter) and then temporally affixed or 'crimped' (i.e., plastically deformed) onto the inflatable balloon portion of catheter forming the stent delivery system. Upon insertion into the in vivo vascular environment, the delivery system must be manipulated within the tortuous anatomical pathways leading to the a priori targeted vessel. Deployment of the stent into the artery is accomplished by gradual inflation of the balloon portion of the delivery system via manually applied hydraulic pressurization, thereby inducing expansion (via plastic deformation), into the neointimal lumina of the targeted site. Upon reaching the intended deployment diameter, the balloon catheter is removed by first deflation and then extraction of the deflated delivery system through the vasculature. The final step occurs during deflation when the Hookean stent material elastically recoils to a smaller diameter, which is also influenced by endoluminal loading imparted onto the deployed stent. The subsequent cyclic loading is then provided by cyclic systolic/diastolic pressurization due to cardiac heartbeats.

To perform the numerical stress-analysis for cyclic radial loading, the stent was modeled with three-dimensional 8-node brick "reduced-integration" elements using ABAQUS/Explicit finite-element code [7]. Five stent "columns" were modeled to ensure that stress variation along the length of the stent was adequately captured. To keep the analysis run-time reasonable, a finite-element mesh consisting of three elements along the stent wall thickness direction and five along the width of any given feature was used. Mesh convergence analyses with this mesh density showed negligible error when compared with a finer mesh, for this specific design and overall treatment.

The loading on the stents was modeled in terms of the several discrete modes that they experience in service, namely (i) assembly, (ii) balloon-inflation, (iii) recoil, and physiological loading within the artery, as described below.

During the first step of the simulation, the stent was crimped to simulate the assembly of the stent onto the balloon catheter. This was accomplished by modeling contact between the stent outer surface and a semi-rigid crimp cylinder (Fig. 1). The nodes on the "semi-rigid" crimp cylinder were constrained axially as well as circumferentially on a cylindrical coordinate system oriented along the stent longitudinal axis. Boundary conditions were imposed to radially contract the crimp cylinder, thereby crimping the stent to the desired profile.

At the end of the crimp step, a semi-rigid expansion cylinder was used to expand the stent to an internal diameter of 3.5 mm (Fig. 1). This step simulated the controlled inflation of the balloon (underlying the stent), driving the stent to expand to the desired expansion diameter. This expansion was performed into a simulated hyper-elastic tube with an initial diameter of 3.25 mm. The hyper-elastic tube represented the section of the coronary artery into which the stent is implanted. The stent expansion step was accomplished by modeling contact between the expansion cylinder and the stent as well as between the stent and the internal surface of the tube. For this specific treatment, the material constants of the hyper-elastic tube were numerically calibrated at the onset of the analysis to exhibit a physiologically relevant coronary arterial distension of 6%[2] for a conservative pressure range on the order of 100 mmHg.

After the expansion step, the stent/tube system was allowed to recoil by retracting the expansion cylinder. This step simulated the balloon deflation and retraction of the balloon catheter. Maximal and minimal pressure loads bounded by the 100 mmHg pressure range, were then sequentially applied to the internal faces of the tube to conservatively represent physiological systolic and diastolic blood-pressure loads within the artery. It was observed that increasing internal pressure loads (from diastolic to systolic values) incrementally counteracted the stent/tube contact forces, thereby slightly reducing the peak stent stresses. The stent material response was found to be linear-elastic during the fatigue cycle. The maximum principal stress distribution across the stent for the two pressure load steps was used to predict a fatigue safety factor (FSF), as explained in Section 4.

4. Stress/life (S/N) predictions

The stress amplitude versus life (S/N) curve for the L-605 Co–Cr stent material was characterized to determine the fatigue endurance strength ($\Delta\sigma_e/2$) (or "fatigue limit") under conditions of zero mean stress (σ_m), i.e., at a load ratio of $R = -1$ (Fig. 2). The endurance strength was experimentally measured as the stress amplitude ($\Delta\sigma/2$) to yield a life of 4×10^8 fatigue cycles or greater. Testing was performed in 0.9% saline solution at 37 °C on 125 μm diameter wire specimens using rotary-beam fatigue-testing machine, operating in displacement control at a frequency of 60 Hz under stress amplitudes ranging from 200 to 625 MPa. From these results (Fig. 2), the 4×10^8 cycle endurance strength of the Co–Cr alloy was determined to be $\Delta\sigma_e/2 = 207$ MPa.

For the two pressure loads discussed in Section 3, the mean stress (σ_m) and stress amplitude ($\Delta\sigma/2$) distributions were calculated from the predicted maximum principal stresses across the stent (Fig. 3). The predicted stress amplitudes and mean stresses were then used to calculate a "FSF" distribution by utilizing the modified-Goodman relationship [8]. The "FSF", which essentially quantifies the proximity of the mean stress and stress amplitude at any given numerical integration point to the limiting Goodman curve (Fig. 3), was determined as $1/FSF = (\sigma_m/\sigma_u) + (\Delta\sigma/2)/(\Delta\sigma_e/2)$. Here σ_u and $\Delta\sigma_e/2$ represent, respectively, the true stresses associated with the ultimate

[2] If d^i_{min} and d^i_{max} are the tubing internal diameters under minimum and maximum pressures and $d^i_{avg} = (d^i_{min} + d^i_{max})/2$, then distension is defined as $(d^i_{max} - d^i_{min})/d^i_{avg}$.

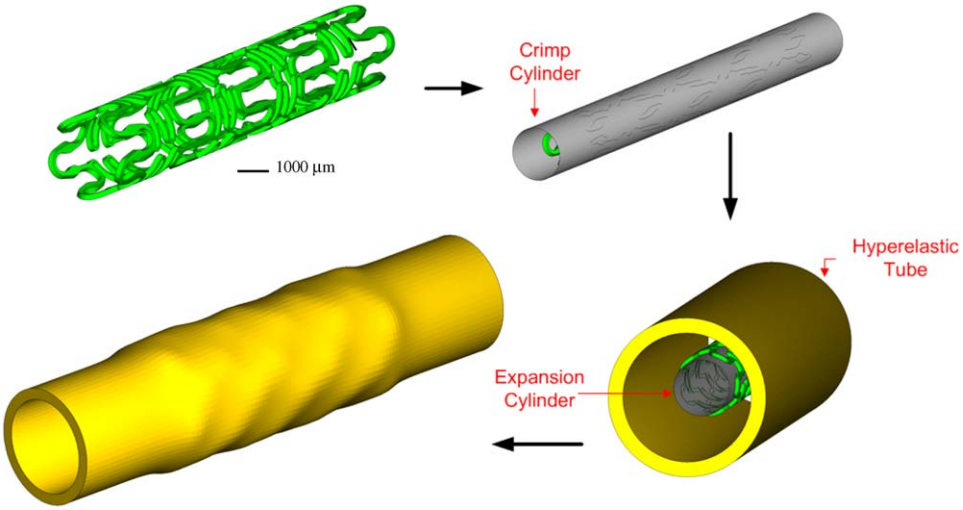

Fig. 1. Schematic of the sequence used to assemble and deploy the stent involving the crimp and expansion steps modeled by the stress analysis.

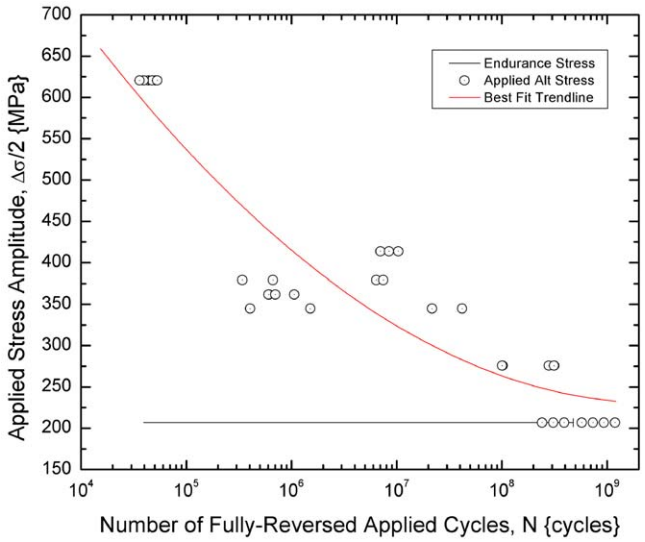

Fig. 2. Stress amplitude vs. number of cycles (S/N) fatigue data for 125-μm diameter wire specimens of L-605 alloy, tested in rotary bending at $R = -1$ in 37 °C 0.9% saline solution at 60 Hz.

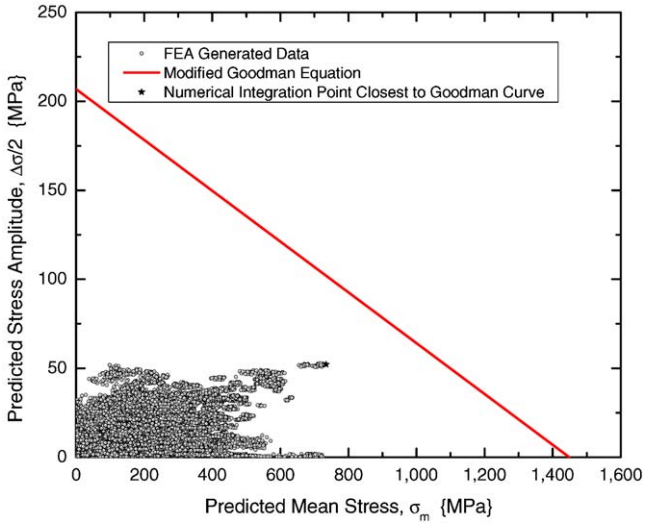

Fig. 3. Comparison of predicted mean stresses and stress amplitudes with the modified Goodman curve. The numerical integration point with coordinates (735, 52) MPa is closest to the Goodman curve and represents the worst-case fatigue region.

tensile strength and endurance strength of the Co–Cr stent material; actual values used in the current analysis are listed in Table 1. A contour plot of the inverse of *FSF* depicting the zone with the maximum inverted value or the lowest *FSF*, is shown in Fig. 4. The mean stress, stress amplitude, and *FSF* for the worst-case fatigue location (element with the lowest safety factor) are listed in Table 2.

5. Role of cracks

To investigate the role of microstructural anomalies, e.g., flaws or cracks, in the stent material and how this might affect the performance and reliability of the stent, a damage-tolerant analysis was performed on the expanded stents utilizing linear-elastic fracture mechanics. To quantify the dimensions of typical defects, stent samples were selected from batches that were either in their laser-cut configuration or those that were over-expanded to an inner diameter of 4 mm (stents were actually designed for an expansion diameter range of 2.5–3.0 mm). The high stress/strain regions, as defined from the stress analysis described above, were inspected under a scanning electron microscope (SEM). Sites with flaws were identified and sectioned for measurement of crack depths. This was performed using a combination of field-emission (FE–SEM) and focused-ion beam (FIB) microscopy, which enabled real-time high-resolution imaging of a stent section during the process of micro-milling, from which accurate crack-depth measurements could be made.

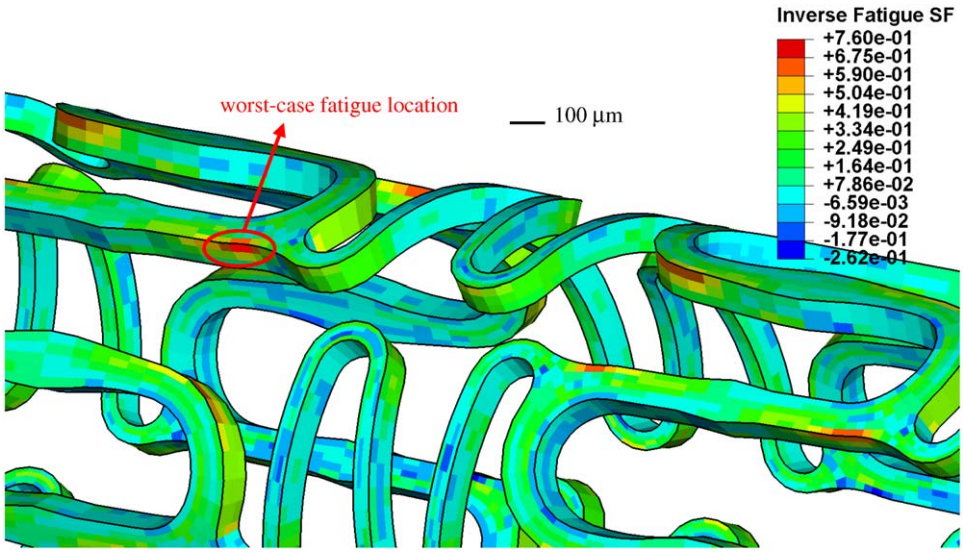

Fig. 4. Contour plot of inverse fatigue safety factors, showing worst-case fatigue location where fatigue cracks are most likely to initiate.

Table 2
Stresses and fatigue safety factor at worst-case fatigue location

Max. principal stress at systolic pressure (MPa)	Max. principal stress at diastolic pressure (MPa)	Mean stress σ_m (MPa)	Stress amplitude $\Delta\sigma/2$ (MPa)	Inverse fatigue safety factor ($1/FSF$)	Fatigue safety factor (FSF)
683	787	735	52	0.76	1.32

Table 3 lists the depth and the corresponding depth-to-length ratios of small cracks detected in two unexpanded and two expanded stent samples. It was observed that the microstructural anomalies were associated either with grain boundaries or generated during fabrication, e.g., as an unintended consequence of ultrasonic agitation during processing. To conservatively characterize the shape of such flaws, a depth-to-surface-length ratio of $c/2a \sim 0.33$ was assumed; this shape was used to represent the flaw-geometry while predicting the stress-intensity factors. SEM and FE–SEM images of one of the fracture sites are shown in Fig. 5. Flaws as large as 92 μm were intentionally developed using excessive ultrasonic agitation to enable large range of crack sizes to be studied. Such large flaws are unlikely to be observed in production stents.

5.1. Stress-intensity solutions

To characterize the severity of these defects under typical in vivo loading conditions, stress-intensity solutions were computed in terms of the Mode-I, -II and -III stress-intensity factors, K_I, K_{II} and K_{III}, respectively, as a function of crack length.[3] To facilitate this, cracks of differing lengths were introduced in the vicinity of the most fatigue-prone location of the stent, as depicted in Fig. 4. The cracks were introduced in the post-expanded state of the stent and examined under three different loading sequences, specifically stent recoil or springback, aforementioned systolic and diastolic loading.

Finite-element model for fracture analysis: To evaluate postulated flaws in post-expanded stents, a fracture-mechanics-based numerical model was developed. The goal of this model was to predict stresses locally in the stent region containing the flaw. Therefore it was undesirable and computationally inefficient to model the entire stent for the fracture mechanics study. A "submodeling" capability of the ABAQUS finite-element analysis program was utilized, which allowed for a localized region of the stent structure to be modeled in a greater level of detail based on the numerical results from the entire stent analysis. The initial fatigue evaluation for the unflawed stent structure was performed with ABAQUS/Explicit as described in Section 4. A follow-on analysis on a detailed

[3]The stress-intensity factor, K, is a measure of the magnitude of the local stress and displacement fields in the vicinity of a crack tip in a linear-elastic solid. It can be computed globally in terms of relationships such as $K = Q\sigma_{app}(\pi a)^{1/2}$, where σ_{app} is the applied far-field stress, a is the crack length, and Q is a function (of order unity) of crack size and geometry, and applied under nominally linear-elastic, so-called small-scale yielding, conditions. The fracture toughness, K_c, is then the critical value of the stress intensity K for unstable fracture at a pre-existing crack. Values of K and K_c can be determined for the three modes of crack displacements, namely tensile opening (Mode I), shear (Mode II) and anti-plane shear (Mode III), although most cracks fail in Mode I.

Table 3
Microcrack geometry as measured from unexpanded and expanded stents

	Anomaly type/location	Crack depth (c)	Crack length ($2a$) (μm)	~Depth to length ratio ($c/2a$)
Expanded sample #1	Grain-boundary separation	970.8 nm	15.2	0.06
Expanded sample #2	Grain-boundary separation	545.1 nm	4.7	0.12
Unexpanded sample #1	Ultrasonic cracks	33.9 μm	91.8	0.37
Unexpanded sample #2 (site A)	Ultrasonic cracks	6.9 μm	52.4	0.13
Unexpanded sample #2 (site B)	Ultrasonic cracks	3.4 μm	52.4	0.07
Unexpanded sample #2 (site C)	Ultrasonic cracks	14.8 μm	64.5	0.23

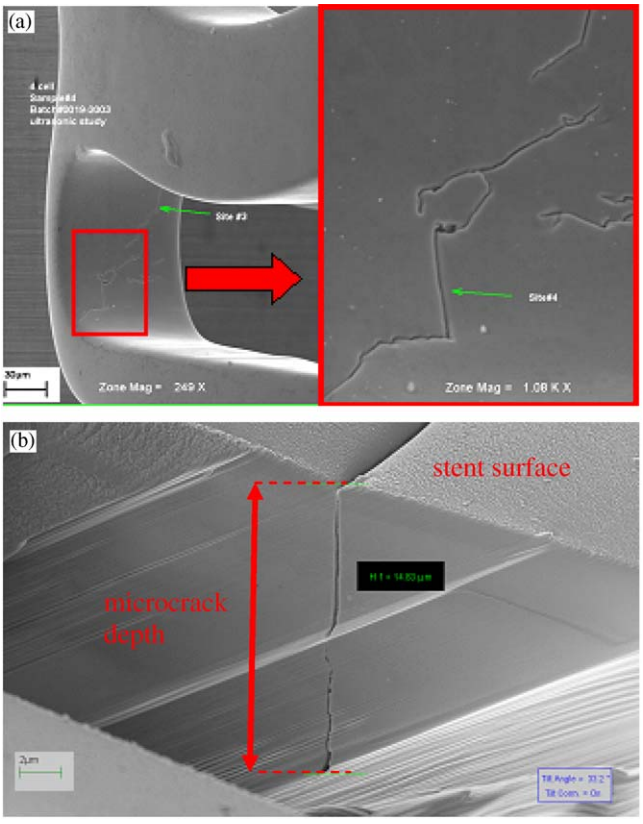

Fig. 5. Scanning electron microscopy of an unexpanded stent sample: SEM image showing processing-induced flaw (a) and zoomed in FE–SEM image of cut section showing crack depth (b).

submodel of the worst-case fatigue region (Fig. 6) was then run with ABAQUS/Standard.

The submodel consisted of a mesh of quadratic elements and was generated without a postulated flaw in order to refine and/or verify the initial fatigue analysis results. The flaw in the submodel was represented with quarter-point element (QPE) 20-noded bricks. The submodel analysis imposed the displacement profile obtained from the full stent model onto the boundaries of the submodel. This enabled the calculation of the stress intensities, K_{I}, K_{II} and K_{III}, using the "interaction-integral" method [9]. From the predicted stress intensities, an estimate of the J-integral value was computed, based upon the following relationship [10]:

$$J = K_{\mathrm{I}}^2/E' + K_{\mathrm{II}}^2/E' + K_{\mathrm{III}}^2/2G, \quad (1)$$

where G is the shear modulus, and $E' = E$, Young's modulus, under plane-stress loading conditions, and $E/(1-\nu^2)$ in plane strain (ν is Poisson's ratio).[4] J-integral values were also computed directly in ABAQUS/Standard using the "virtual crack extension/domain integral method". The J-integral value was compared to that derived from the K values; a minimal difference (<5%) between these two estimates of J was used as an indicator of adequate mesh refinement and that nominal small-scale yielding conditions prevailed.

Types of flaw modeled: To assess the worst-case conditions in the stent, two types of flaws were studied: a semi-elliptical surface crack, which is most likely to be encountered, and a corner flaw, which can be more prone to inducing structural instabilities as opposed to the former. The first of these were flaws aligned (and centered) solely along the stent wall, as shown in Fig. 6; these *center flaws* were assumed to be semi-elliptical in cross-section with a depth-to-length ($c/2a$) ratio of 0.33. This depth-to-length ratio was chosen to approximately represent the worst-case shape of cracks detected experimentally in actual stents (Table 3). The second type involved *corner flaws* that orientated through and past the edges of the stent structure (Fig. 7). For this case, the effect of edge rounding was included in the finite-element model; edge-radii of 13 and 17 μm were assumed, based on experimental measurements of stent cross-sections. For the corner-flaw, the length of the flaw along the stent wall dimension was designated as a_{w} and length of flaw along the width dimension as a_{f}, where for ease of modeling, $a_{\mathrm{f}} = 2a_{\mathrm{w}}/3$. The secant length of the corner-flaw was assumed to be the effective flaw length ($2a_{\mathrm{eff}}$), as shown in Fig. 7.

The computed stress-intensity factors for the center-flaw geometry, specifically for stent springback, diastolic and systolic loading, are listed in Table 4. Even though these flaws were geometrically centered along the stent wall dimension, a local stress-gradient along the wall thickness resulted in asymmetric stress-intensity factors. The table lists the largest stress-intensity factor along the crack front, which coincided with the location where the crack front

[4]Akin to the stress-intensity factor in a linear-elastic solid, J is a measure of the magnitude of the local stress and displacement fields in the vicinity of a crack tip in a nonlinear-elastic solid, and as such can be used to characterize the onset of failure. It can be computed globally in terms of the rate of change in potential energy with unit increase in crack area.

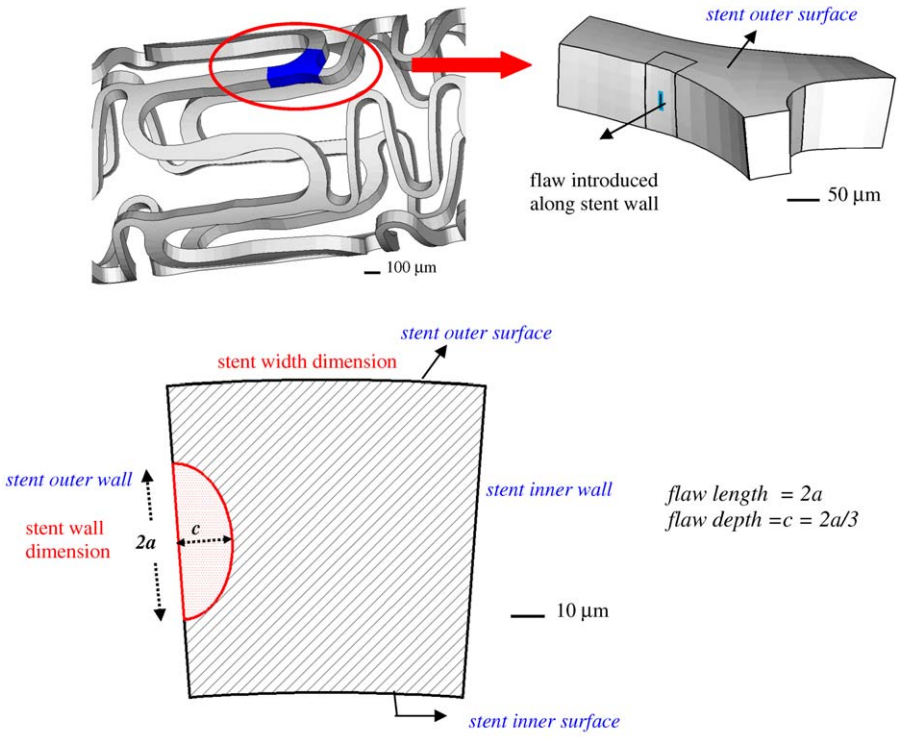

Fig. 6. Geometry for center-flaws oriented along stent wall thickness (radial dimension).

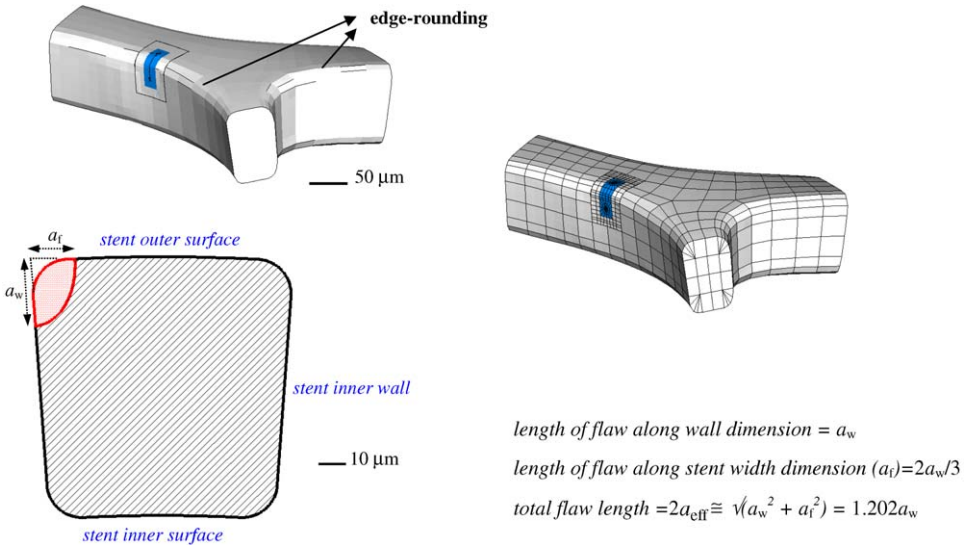

Fig. 7. Geometry of corner-flaws oriented at the stent wall corners.

intersected the free surface of the stent. It should be noted that relative to Mode I values, the Modes II and III stress-intensity factors were negligible, indicating that the tensile stresses along the outer wall of the stent are the dominant stresses influencing failure.

Among the three loading steps that were analyzed, the highest (peak) stress intensity was developed during springback. This can be attributed to internal pressure loads relieving the stent/tube contact forces thereby reducing the tensile crack-opening stresses along the outer wall dimension of the stent. In terms of the simple expression for the stress intensity, i.e., $K_I = Q\sigma_{app}\sqrt{\pi a}$, the geometric factor Q was determined to be 0.624, based on the far-field tensile (crack-opening) stresses at the center of wall dimension. The differences in the stress intensities during diastolic and systolic loading were much smaller; this difference, however, provides the driving force for possible fatigue-crack growth during in vivo loading. Comparable stent stresses were computed during balloon inflation, but these were not considered in such detail as

they occurred in locations other than the most fatigue-prone locations.

Corresponding stress-intensity factors for the corner-flaw geometry were computed and similar to center-flaw results, the highest stress intensities were developed during springback. Additionally, the stress-intensity factors were dominated by the Mode I crack-tip displacements; for equivalent flaw sizes, the largest stress-intensity factor occurred at the outer-wall location. Fig. 8 illustrates the typical stress distribution along the crack-front for the corner flaw geometry. The geometry factor for these corner flaws was found to be $Q = 0.694$.

5.2. Fatigue-crack growth rates

Under fatigue loading conditions, growth of a pre-existing crack can occur at stress-intensities below the fracture toughness of the material. This effect can be described by a Paris power-law formulation [11] for an elastic material under conditions of small-scale yielding at the crack tip. In its simplest form, this law relates the crack-growth increment per cycle (da/dN) to the range of stress intensity during the fatigue cycle (ΔK), viz:

$$\frac{da}{dN} = C(\Delta K)^m, \tag{2}$$

where C and m are experimentally determined scaling constants, N is the number of fatigue cycles, and the stress-intensity range is defined as:

$$\Delta K = \left|K_{\text{systolic}} - K_{\text{diastolic}}\right|. \tag{3}$$

Here K_{systolic} and $K_{\text{diastolic}}$ represent the values of K at the end of systolic and diastolic pressure cycles, respectively, such that $K_{\text{systolic}} = Q\sigma_{\text{systolic}}\sqrt{\pi a}$ and $K_{\text{diastolic}} = Q\sigma_{\text{diastolic}}\sqrt{\pi a}$. At very low growth rates approaching a lattice spacing per cycle, cracks can effectively be considered to be dormant; this stress-intensity range is referred to as the fatigue threshold, $\Delta K^{\text{o}}_{\text{TH}}$, and is generally operationally defined as the minimum ΔK at a growth rate of $\sim 10^{-8}$ mm/cycle [12]. It should be noted here that computed cyclic plastic-zone sizes [13] were always less than $\sim 2\,\mu$m. Since this is at least an order of magnitude smaller than any section size in the stent, conditions pertain to that of small-scale yielding, such that linear-elastic fracture mechanics and the use of the stress-intensity factor can be presumed to be applicable.

Experimental fatigue-crack growth rate data for L-605 Co–Cr alloy under simulated physiological conditions were obtained from Ref. [1]. These data were generated from tests on large (millimeter-sized or larger) through-thickness cracks in conventional compact-tension $C(T)$ specimens, cycled at various load ratios in 37 °C Ringer's solution at a

Table 4
Computed stress-intensity factors for center-flaws

Flaw length ($2a$) (μm)	Load step	K_{I} (MPa$\sqrt{m}$)	K_{II} (MPa$\sqrt{m}$)	K_{III} (MPa$\sqrt{m}$)	J-Integral (from K's)	J-Integral (direct)
10	Stent recoil	1.35	−0.05	−0.03	6.9	7.0
	150 mmHg pressure	1.05	−0.08	−0.03	4.2	4.3
	50 mmHg pressure	1.23	−0.08	−0.03	5.7	5.8
20	Stent recoil	2.05	−0.07	−0.03	15.9	16.3
	150 mmHg pressure	1.62	−0.14	−0.07	9.8	10.0
	50 mmHg pressure	1.88	−0.10	−0.04	13.2	13.4
38	Stent recoil	3.08	−0.10	−0.05	35.5	36.6
	150 mmHg pressure	2.41	−0.19	−0.09	21.9	22.5
	50 mmHg pressure	2.80	−0.13	−0.07	29.4	30.3
50	Stent recoil	3.76	−0.10	−0.05	52.7	54.3
	150 mmHg pressure	2.93	−0.20	−0.10	32.4	33.3
	50 mmHg pressure	3.42	−0.14	−0.08	43.7	45.0
66	Stent recoil	4.66	−0.11	−0.07	81.1	83.0
	150 mmHg pressure	3.63	−0.21	−0.11	49.5	50.5
	50 mmHg pressure	4.24	−0.15	−0.09	67.3	68.8
94	Stent recoil	6.25[a]	—	—	—	—
	150 mmHg pressure	4.86[a]	—	—	—	—
	50 mmHg pressure	5.68[a]	—	—	—	—
20 (offset towards stent outer surface)	Stent recoil	3.20	−0.03	−0.02	38.2	39.1
	150 mmHg pressure	2.57	−0.07	−0.04	24.8	25.2
	50 mmHg pressure	2.94	−0.04	−0.03	32.4	33.1

Note: Reported values are at the crack front towards the outer wall of the stent.
[a]Values extrapolated from those obtained at other flaw sizes.

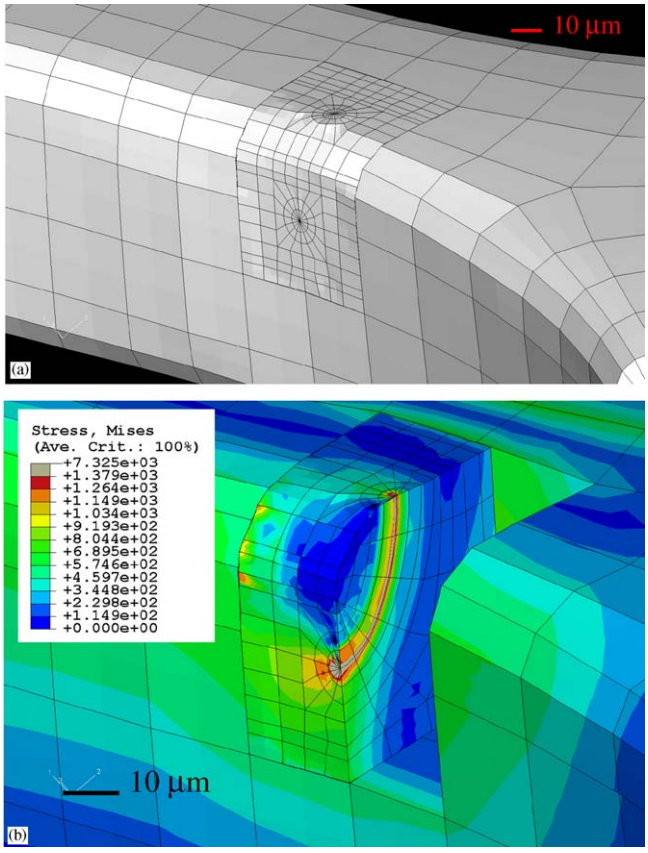

Fig. 8. Finite-element mesh (a) and stress distribution in MPa for 30 μm corner flaw during the recoil (springback) load step (b).

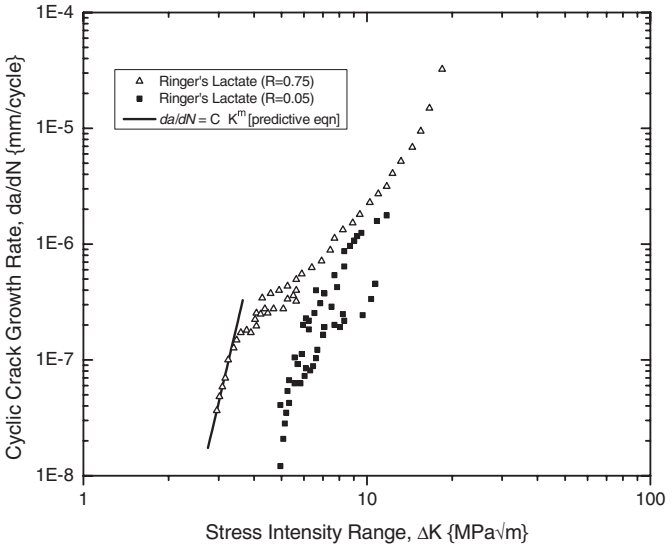

Fig. 9. Variation in fatigue-crack growth rates, da/dN, as a function of stress-intensity range, ΔK, for L-605 alloy under simulated physiological conditions [1].

frequency of 3 Hz close to ΔK^{o}_{TH} and at 30 Hz at larger ΔK values; results at load ratios of 0.05 and 0.75 are plotted in Fig. 9. As the stress analysis described in Section 3 would suggest that the stent experiences load ratios above 0.75 (and as high as 0.90) in the most fatigue-prone regions under physiological conditions, the high load-ratio growth-rate and fatigue threshold data in Fig. 9 were used exclusively for the course of this study. This gives a fatigue threshold of $\Delta K^{o}_{TH} = 2.58\,\mathrm{MPa}\sqrt{m}$ for millimeter-sized cracks. Such use of available $R = 0.75$ data to describe behavior at somewhat higher load ratios is considered to be a reasonable approximation. Extensive results on metallic alloys have shown that above a critical load ratio of typically 0.5, growth rates (in the mid-range and near-threshold regimes) tend to remain unchanged with R; moreover, modeling and experimental results (involving the role of crack closure [14,15]) clearly show that the value of the ΔK^{o}_{TH} fatigue threshold invariably remains constant with increasing R above this critical load ratio.

5.3. Damage-tolerant criteria for failure

The inevitable presence of crack-like flaws within a component such as a stent clearly raises the potential for unexpected fatigue failure or in extreme circumstances, outright fracture. With conventional stress/life analyses, it is difficult to evaluate what effect such flaws might have. However, fracture mechanics provides a powerful methodology to assess the quantitative severity of flaws in terms of their potential for reducing the safe life of the stent. The first step is to compare the stress intensities calculated as a function of crack size for the various loading steps (Table 4) with the limiting stress intensities for failure. Specifically, to prevent overload fracture, the highest peak stress intensity during springback must be less than the fracture toughness, K_c; to prevent fatigue-crack initiation and growth, the stress-intensity range based on the difference in the systolic and diastolic pressures must be less than the fatigue threshold, ΔK^{o}_{TH}.

To consider first outright fracture, from Table 4, the maximum peak stress intensity developed during springback was calculated to be $6.25\,\mathrm{MPa}\sqrt{m}$ for a 94 μm center crack, representing the largest possible (full through-thickness) flaw.[5] This is to be compared with the fracture toughness of the Co–Cr alloy, which under plane-strain conditions is $\sim 60\,\mathrm{MPa}\sqrt{m}$, and would be considerably higher for the more likely plane-stress conditions appropriate to the thin section of a stent. The fact that the toughness is so much higher than the peak stress intensity developed ahead of a crack in excess of 90 μm during implantation and in vivo loading of the stent is a strong indication that outright fracture of the stent from pre-existing defects is a highly unlikely event. This conclusion is further substantiated when inspection procedures are directed as part of a quality control plan to detect and reject all stents containing surface cracks of this magnitude.

[5]Similar stress intensities were estimated during stent expansion, but as stated above, these occurred for cracks in non-critical, i.e., not fatigue-prone, locations on the stent.

Pre-existing cracks, however, can propagate by fatigue during in vivo loading due to the cyclic stresses developed by the difference in the systolic and diastolic pressures. To assess this possibility, the stress-intensity range ΔK, defined in Eq. (3), must be compared with the ΔK^{o}_{TH} fatigue threshold, which under appropriate conditions is $2.58\,\mathrm{MPa}\sqrt{\mathrm{m}}$. The ΔK values for a range of center-crack sizes up to 94 μm are plotted in Fig. 10, and indicate a maximum ΔK of $0.82\,\mathrm{MPa}\sqrt{m}$ for the largest flaw size. Clearly, as this is more than a factor of three times smaller than the fatigue threshold, the propagation of any flaw in the stent smaller than ~90 μm is not likely. Both these estimates imply that provided all stents containing surface flaws in excess of 90 μm are detected, premature failure due to balloon deflation or in vivo radial fatigue will not occur.

5.4. Role of small cracks

Although correct in principle, one problem with the approach so far is the physically small size of stent components, which means that the crack sizes under consideration will also be physically small in dimension. This is important because it is known that when cracks become small compared to (i) the scale of microstructure, (ii) the extent of local crack-tip plasticity, or (iii) the extent of crack-tip shielding in the wake of the crack, they can propagate at stress intensities below the fatigue threshold (as measured for larger cracks) and at growth rates in excess of those of large cracks at comparable stress intensities [3,4,16]. Typically, the crack size below which such "small crack effects" become significant can be estimated by determining a transition (surface) crack size, $2a_o$, based on the ΔK^{o}_{TH} threshold stress intensity and the endurance strength (expressed as a stress amplitude and corrected for the appropriate R ratio), $\Delta\sigma'_e/2$ [16]:

$$2a_o \sim \frac{2}{\pi}\left(\frac{\Delta K^{o}_{TH}}{Q\Delta\sigma'_e}\right)^2. \quad (4)$$

However, in terms of the variation in limiting stress (i.e., endurance strength) and stress intensity (i.e., fatigue threshold) for fatigue failure, it is also known that conventional stress/life fatigue and fracture mechanics based threshold measurements [13] show that at a specific load ratio:

- for small flaws (where $2a \leqslant 2a_o$), the endurance strength, $\Delta\sigma'_e/2$, is constant, whereas
- for large flaws (where $2a \geqslant 2a_o$), the fatigue threshold, ΔK^{o}_{TH}, is constant.

In fracture mechanics terms, these observations translate into the fact that the fatigue threshold will be progressively decreased below the large-crack ΔK^{o}_{TH} value with decreasing crack sizes less than $2a_o$. Accordingly, it is necessary to estimate the value of this transition crack size and to deduce how ΔK_{TH} varies with a for $2a \leqslant 2a_o$. For the current material, stent design, loading and crack configurations, values of $2a_o$ can be estimated from Eq. (4) to be 262 μm for center-flaw geometry and 212 μm for the assumed corner-flaw geometry. As these transition flaw sizes are well above the typical crack dimensions within the fatigue-prone regions, it is clear that all center or corner flaws being addressed in this analysis predominantly fall into the "small-flaw" category.

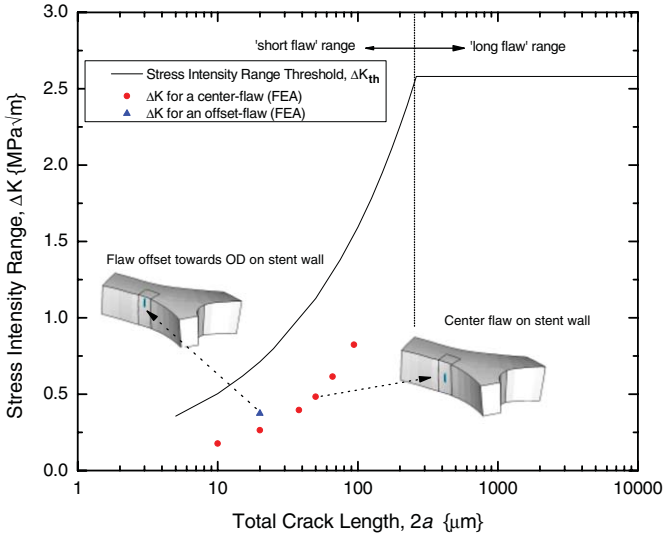

Fig. 10. Predicted stress-intensity ranges, ΔK, for center-cracks as a function of surface crack size, $2a$.

For large cracks, we have reasoned that no crack growth leading to fatigue failure is likely to occur provided:

$$\Delta K \leqslant \Delta K^{o}_{TH} \text{ and } \Delta\sigma/2 \leqslant \frac{\Delta K^{o}_{TH}}{2Q\sqrt{\pi a}}. \quad (5)$$

Now for small cracks, these corresponding criteria become:

$$\Delta K \leqslant \Delta K_{TH}(a) \text{ and } \Delta\sigma/2 \leqslant \Delta\sigma'_e/2,$$

where

$$\Delta K_{TH}(a) = Q\Delta\sigma'_e\sqrt{\pi a} \text{ and } \frac{\Delta\sigma'_e}{2} = \frac{\Delta\sigma_e}{2}\left(1 - \frac{\sigma_m}{\sigma_u}\right). \quad (6)$$

Here $\Delta\sigma'_e/2$ is the endurance strength adjusted for the appropriate mean stress, σ_m (or load ratio), using the Goodman relationship, where σ_u is the ultimate tensile strength.

Results comparing these limiting conditions, expressed in terms of the variation of fatigue threshold with crack size, with the typical stress-intensity ranges experienced by representative center and corner cracks in the stent under peak in vivo loading are shown in Figs. 10 and 11, respectively. Results show that despite the "small crack effect", stress intensities, developed for representative crack configurations in fatigue-prone locations in the stent under anticipated peak in vivo loading, are still less than the threshold stress intensity ranges for fatigue failure, for crack sizes ranging from 10 μm up to a maximum possible crack size of ~90 μm. On the basis of this, once again, we

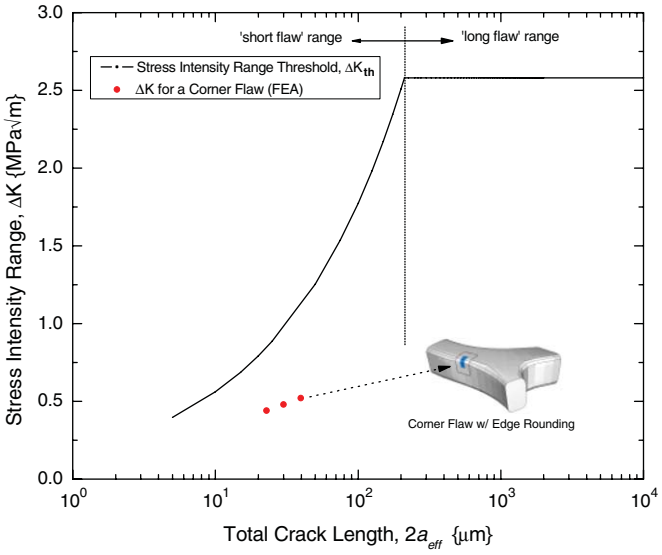

Fig. 11. Comparison of the computed ΔK values with the ΔK_{TH} threshold stress-intensity values for corner-flaws in the large and small crack regimes.

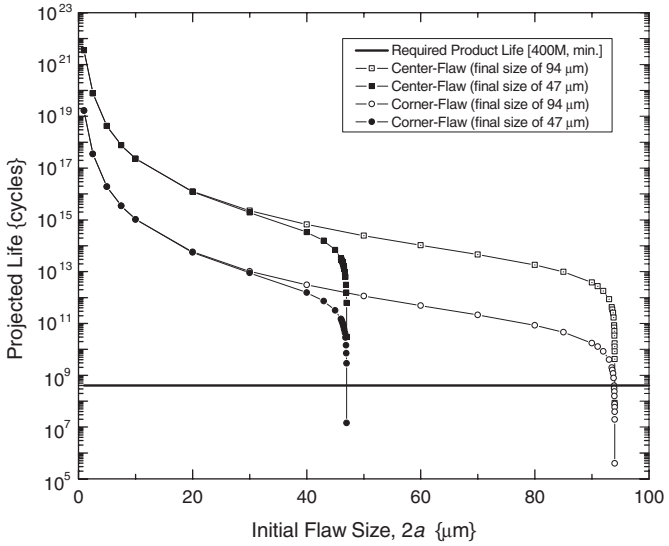

Fig. 12. Conservative predictions of the lifetime of the stent under in vivo pulsatile radial loading as a function of pre-existing flaw size (for center- and corner-cracks). On the assumption of 40 million loading cycles per year, it can be seen that predicted lives well exceed the required design life of 10 patient years (4×10^8 cycles), except where $2a \rightarrow 2a_f$.

can conclude that provided no stents contain cracks in excess of this latter dimension, premature fatigue failure due to radially pulsatile physiological loading is unlikely to occur.

5.5. Damage-tolerant life predictions

The analysis described above demonstrates that computed stress-intensity ranges for practical flaw sizes are less than the threshold values for radially pulsatile in vivo loading. A more conservative approach can be achieved by making no assumption concerning the existence of a fatigue threshold (this presumes infinitesimally small crack-growth rates for the flaw sizes in question) and then integrating the fatigue-crack propagation relationship in Fig. 9 between the limits of the initial and final crack size for the fatigue-prone regions; in such a way, predictions of a finite lifetime for the stent can be deduced as a function of pre-existing flaw size. In the present analysis, to preserve a conservative approach, the Paris-law scaling constants in Eq. (2) were derived by a regression fit to the near-threshold fatigue-crack growth data only,[6] as shown in Fig. 9; values (in units of mm/cycle and MPa$\sqrt{m}$) of $C = 4.74 \times 10^{-13}$ and $m = 10.39$ were obtained.

The integration was achieved by substituting the appropriate K solutions into the Paris law formulation (Eq. (2)), and integrating between an initial crack size ($2a_i$), indicative of the pre-existing flaws in the stent, and the final crack size ($2a_f$), indicative of stent fracture, to give the number of loading cycles to failure, N_f:

$$\int_0^{N_f} dN = \frac{1}{C\pi^{m/2}} \int_{a_i}^{a_f} \frac{1}{Q^m (\Delta\sigma)^m a^{m/2}}\, da, \tag{7a}$$

such that:

$$N_f = \frac{2}{C(m-2)Q^m(\Delta\sigma)^m \pi^{m/2}} \left[\frac{1}{a_i^{(m-2)/2}} - \frac{1}{a_f^{(m-2)/2}} \right]. \tag{7b}$$

It should be noted that Eq. (7b) is derived on the assumption that the stress amplitude, $\Delta\sigma/2$, and the K-solution, specifically the value of Q, do not change between these flaws lengths; in view of the small flaw sizes involved, this is clearly a realistic assumption.

Predicted lifetimes for the stent under in vivo pulsatile radial loading are plotted in Fig. 12 as a function of the pre-existing flaw size for center-flaw and corner-flaw geometries. On the assumption of 40 million loading cycles per year, i.e., a heart rate of 1.2 Hz, it can be seen that predicted lives well exceed the required design life of 10 patient years (4×10^8 cycles), except where pre-existing crack sizes approach $2a_f$. The choice of final crack size, representing device failure, thus dictates where the projected life approaches the required design life. In the present study, we have conservatively chosen a final crack size of roughly 90 μm, i.e., a crack spanning the full thickness of the stent. Provided all flaws smaller than this size are detected prior to the stent entering service, projected lives will be far in excess of patient lifetimes.

6. Limitations of the analysis

The fracture mechanics based, damage-tolerant methodology performed in this work for a cardiovascular stent

[6] This is deemed to be a reasonable and conservative approach as, on the basis of the K calculations for in vivo pulsatile loading (Figs. 10 and 11), ΔK values for all relevant flaw sizes, i.e., up to 94 μm, are less than 2 MPa$\sqrt{m}$.

has several important features. Although we believe that it should be supplementary to conventional (e.g., stress/strain-life) analysis (and not necessarily replace it), the proposed damage-tolerant approach is inherently more conservative and is based on the critical concept of *testing to failure*, rather than for survival. Moreover, unlike stress/strain-life approaches, it provides for a *quantitative* evaluation of the potential effect of flaws, which inevitably may be present in the fabricated stent. However, in general terms, there are still certain limitations in the approach which may need to be addressed, particularly in situations where projected lives approach the design lives, e.g., in components where there is a greater probability of finding larger pre-existing defects and/or where the *in service* stresses are higher. These limitations primarily pertain to the estimation of the in vivo stresses and in the determination of fatigue-crack growth rate and threshold behavior for the material/component in question.

Firstly, with respect to the stress analysis, it is important to realize that there is always a potential problem with physically small components that continuum finite-element calculations may not be totally applicable. For example, there may be situations where the stent struts and wall dimensions, which are typically in the range of ~75–150 μm for coronary stents, are comparable to the characteristic scale of the microstructure, e.g., the grain size; in these situations, continuum approaches relying on macroscopic material properties to model material behavior may be regarded as somewhat questionable, and alternative numerical analyses, based on crystal plasticity for example, may need to be employed. Additionally, some assessment of the residual stresses in the material is always beneficial. In the present case, where the stent component is plastically deformed during deployment, the residual stress state in the starting material would not be that important to the in vivo state of stress, but in other implant devices, it may represent a large component of the stress that the device must endure.

Secondly, the fatigue threshold and growth-rate data used to predict lifetimes should ideally be measured on material that is truly representive of the finished component. In the present case, this would necessitate measuring growth rates of small cracks with dimensions in the tens of micrometers in ~200 μm wide components, which is a difficult proposition. However, one approach might be to assess the growth rates on the tubular material used to laser cut the stents; in a parallel study [17] on fatigue-crack growth in Nitinol stents, small compact-tension samples have been successfully cut from such tubes after they had been cut open and straightened. The conditions under which these tests are conducted are also of importance; for the current stent application they should be performed at high load ratios and in a simulated physiological environment.[7] Finally, although well beyond the scope of the present work, some assessment of the effect of mixed-mode loading would be worth considering, particularly as in stents, in vivo conditions may involve loading conditions such as torsional, axial loading and dynamic bending in addition to the radially pulsatile loading addressed in this treatment.

7. Conclusions

In this work, fracture mechanics based analyses have been used to estimate conservative lifetimes and to quantitatively assess the severity of pre-existing flaws in a coronary stent, fabricated from the Co–Cr alloy, L605. The approach, which relies on (i) finite-element computations of the stresses and stress-intensity factors for worst-case flaws and (ii) experimental fatigue testing to failure, involving both conventional stress/life and crack-propagation rate measurements, is applied to the principal loading sequences of stent deployment and subsequent radially pulsatile in vivo cycling, with special consideration made of the role of physically small cracks. It is shown that for the stent in question, provided all flaws greater than ~90 μm are detected prior to the device entering service, premature in vivo fatigue failure due to radially pulsatile physiological loading is highly unlikely to occur.

Acknowledgments

This work was supported by internal funding from Cordis Corporation, a Johnson & Johnson company. The authors wish to thank Dr. Chao Chen and Dr. Tim Kiorpes for their encouragement and ongoing support. In addition, the authors are indebted to Dr. Tom Duerig, Nitinol Devices & Components, a Johnson & Johnson company, for his insightful guidance and assistance during the development of this manuscript. The authors also wish to acknowledge Ms. Robin Ratkowski for conducting significant microcopy efforts in support of this work.

References

[1] Ritchie RO, Lubock P. Fatigue life estimation procedures for the endurance of a cardiac valve prosthesis: stress/life and damage-tolerant analysis. J Biomech Eng 1986;108:153–60.
[2] Ritchie RO. Fatigue and fracture of pyrolytic carbon: a damage-tolerant approach to structural integrity and life prediction in "ceramic" heart-valve prostheses. J Heart Valve Dis 1996;5–1: S9–S31.
[3] Suresh S, Ritchie RO. The propagation of short fatigue cracks. Int Metals Rev 1984;29:445–76.
[4] Ritchie RO, Lankford J. Small fatigue cracks: a statement of the problem and potential solutions. Mater Sci Eng 1986;84:11–6.

[7] Ideally these experiments should be conducted at a representative in vivo cyclic frequency, i.e., ~1–2 Hz. Unfortunately, this would not permit, (*footnote continued*) in realistic time scales, the measurement of the lowest growth rates, which are so critical to the damage-tolerant analysis. Accordingly, as it is necessary to conduct the fatigue tests at a frequency of typically 30–50 Hz, some independent assessment of whether frequency affects the near-threshold behavior over this range would be a wise course of action.

[5] ASTM Standard E112-96. Standard test methods for determining average grain size.
[6] ASM, Manufacturer's and handbook data, 2004.
[7] ABAQUS Inc., 166 Valley St., Providence, RI, USA
[8] Shigley JE, Mischke CR. Mechanical engineering design, 6th ed. New York: McGraw Hill; 2001.
[9] Analysis user manual, ABAQUS version 6.5, 2004; II-7.10.2
[10] Shih CF. Relationship between the *J*-integral and the crack opening displacement for stationary and extending cracks. J Mech Phys Solids 1981;29:305–26.
[11] Paris PC, Erdogan F. A critical analysis of crack propagation laws. J Basic Eng Trans ASME Ser D 1960;85:528–34.
[12] ASTM Standard E647-93. Standard method for the measurement of fatigue crack growth rates. In: Annual book of ASTM standards. West Conshohocken, PA: American Society for Testing and Materials; 2001.
[13] Suresh S. Fatigue of materials. 2nd ed. Cambridge, UK: Cambridge University Press; 2001. pp. 544–547.
[14] Schmidt RA, Paris PC. Threshold for fatigue crack propagation and the effects of load ratio and frequency. In: Progress in flaw growth and fracture toughness testing, ASTM STP 536. Philadelphia, PA: American Society for Testing and Materials; 1973. p. 79–94.
[15] Suresh S, Ritchie RO. On the influence of environment on the load ratio dependence of the fatigue threshold in pressure vessel steel. Eng Fract Mech 1983;18:785–800.
[16] El Haddad MH, Topper TH, Smith KN. Prediction of non-propagating cracks. Eng Fract Mech 1979;11:573–84.
[17] Robertson SW, Stankiewicz J, Gong XY, Ritchie RO. Cyclic fatigue of Nitinol. In: Proceedings of the international conference on shape memory and superelastic technologies. Menlo Park, CA: SMST Society, Inc.; 2004.